

# Incompressible Navier-Stokes Computations for a Round-Edged Double-Delta Wing

C.-H. Hsu\* and P.-M. Hartwich†

*Vigyan Research Associates, Inc., Hampton, Virginia*  
and

C. H. Liu‡

*NASA Langley Research Center, Hampton, Virginia*

## Contents

**I**N recent years, several experimental investigations on flows over double-delta wings have been carried out in low-speed wind tunnels,<sup>1,2</sup> in water tunnels,<sup>1</sup> and with towing tanks.<sup>3</sup> More recently, numerical simulations of leading-edge vortices for double-delta wings at low speeds, using different Navier-Stokes solvers, have been reported.<sup>4-6</sup> This synoptic presents the numerical results for a thin double-delta wing.

The double-delta wing with an aspect ratio of 2.05 and a maximum thickness of  $0.006c$  ( $c$  = root-chord length) has a leading-edge kink at  $x/c = 0.5$ , and has 80 and 60 deg sweeps for the leading edges of the strake and the main wing, respectively. All edges of the wing are rounded with radii of one-half the wing thickness. This geometry was studied by Brennenstuhl and Hummel<sup>1</sup> in a low-speed wind tunnel at  $Re_c = 1.3 \times 10^6$  ( $M_\infty \approx 0.1$ ) and in a water tunnel at  $Re_c = 10^4$ .

A C-H grid<sup>6</sup> of 531,765 points is generated plane by plane longitudinally for the test geometry using an elliptic solver. The shape of the computational domain is described by a cylinder with a radius of  $2.5c$ . The grid extends  $1.5c$  upstream of the apex and  $1.5c$  downstream of the trailing edge. The grid is segmented into 81 crossflow planes that are perpendicular to the longitudinal axis of the wing. In each crossplane, there are 65 and 101 grid points in the radial and circumferential directions, respectively. The maximum spacing normal to the wing surface for the first grid line encircling the wing at the trailing edge is  $0.5 \times 10^{-4}c$ . Crossplanes are clustered near the apex, kink, and trailing edge. The minimum spacing between crossplanes is  $1.2 \times 10^{-3}c$ .

The computational method is briefly described. By adding a time derivative of pressure to the continuity equation, the unsteady, incompressible Navier-Stokes equations are integrated like a conventional parabolic time-dependent system of equations.<sup>5-7</sup> A flux-difference splitting based on Roe's approximate Riemann solver<sup>8</sup> is chosen to upwind-difference the inviscid fluxes. Second-order spatial accuracy is achieved by using central differences for the viscous shear fluxes and by applying total-variation-diminishing (TVD)-like discretizations<sup>7</sup> to the inviscid fluxes. The implicit scheme combines approximate factorization in cross planes with a symmetric planar Gauss-Seidel relaxation in the remaining spatial direction. The solutions are advanced in pseudotime using Euler-implicit time differencing. When a steady state is approached,

the artificial time derivative of pressure diminishes, resulting in an incompressible solution.

## Numerical Results

The finite-difference solutions for  $Re = 1.3 \times 10^6$  are carried out in 32-bit word arithmetic on the CDC CYBER 205 vector computer at NASA Ames Research Center. The CPU time per grid point per iteration is  $37.3 \mu s$ . All steady-state solutions are calculated with local time stepping ( $CFL = 10$ ). Within about 750 iterations, the  $L_2$  norms of all residuals are reduced by three orders of magnitude for  $\alpha = 12$  and 20 deg and by nearly two orders of magnitude for  $\alpha = 40$  deg.

Computed total pressure contours at  $x/c = 0.50, 0.55$ , and  $0.95$  for  $\alpha = 12$  deg are shown in Fig. 1. At the kink crossplane ( $x/c = 0.50$ ), both the primary stake vortex and its induced secondary vortex above each half-wing are visible (Fig. 1a). Above the stake, the crossflow pattern is similar to that at the kink crossplane. Downstream of the kink crossplane at  $x/c = 0.55$  (Fig. 1b), an additional vortex, the wing vortex, is clearly indicated. Further downstream, the weaker stake vortex moves downward and outboard and the stronger wing vortex moves upward and inboard. At  $x/c = 0.95$  (Fig. 1c), the two primary vortices have almost merged into one single vortex above each half-wing. Figure 2 shows that the computational and experimental<sup>1</sup> vortical trajectories (local total pressure minima) of the two interacting primary vortices compare quite well with each other.

Figure 3 exhibits the distributions of spanwise surface-pressure coefficients. At  $x/c = 0.55$  (Fig. 3a), the outer wing vortex induces a much higher suction-pressure peak than that of the inner stake vortex. At  $x/c = 0.75$  (Fig. 3b), the predicted levels of suction pressure are lower than the experimental data<sup>1</sup> at  $\alpha = 12$  deg; the locations of the static pressure minima are not accurately predicted either. This discrepancy can probably be attributed to the insufficient crossflow resolution. More resolution is required in the neighborhood of the vortical cores for precise predictions of surface-pressure distribution.

Figure 4 displays the lift variation with the angle of attack for the present full incompressible Navier-Stokes solutions (squares), for Fujii and Schiff's thin-layer compressible Navier-Stokes calculations<sup>4</sup> (triangles), and for Brennenstuhl and Hummel's wind-tunnel data<sup>1</sup> (circles). Both numerical and experimental results indicate that the lift variation is nonlinear with respect to the angle of attack due to the vortex formation, interaction, and breakdown. Fujii and Schiff's computations ( $M_\infty = 0.3$ ) with thousands of iterations were carried out on a grid of 853,349 points. Their predicted lift coefficients compare very well with the experimental data up to  $\alpha \approx 27$  deg; at  $\alpha > 27$  deg their values are underpredicted. In the present calculations ( $M_\infty = 0.0$ ), the asymptotic steady-state lift coefficients are obtained within 600 iterations and they are in good agreement with experimental data over the entire range of angle of attack, the predicted maximum lift coefficient up to but not including  $\alpha = 40$  deg. ( $C_{L_{max}} = 1.20$ ) at  $\alpha = 30$  deg agrees closely with the measured maximum lift coefficient ( $C_{L_{max}} = 1.21$ ) at  $\alpha \approx 27$  deg. Computed results at

Presented as Paper 87-1341 at the AIAA 19th Fluid Dynamics, Plasma Dynamics and Lasers Conference, Honolulu, HI, June 8-10, 1987; Synoptic received March 4, 1988; Full paper available from AIAA Library, 555 W. 57th St., New York, NY 10019. Price: microfiche, \$4.00; hard copy, \$9.00. **Remittance must accompany order.** This paper is declared a work of the U.S. Government and is not subject to copyright protection in the United States.

\*Research Scientist, Senior Member AIAA.

†Research Scientist, Member AIAA.

‡Senior Research Scientist, Senior Member AIAA.

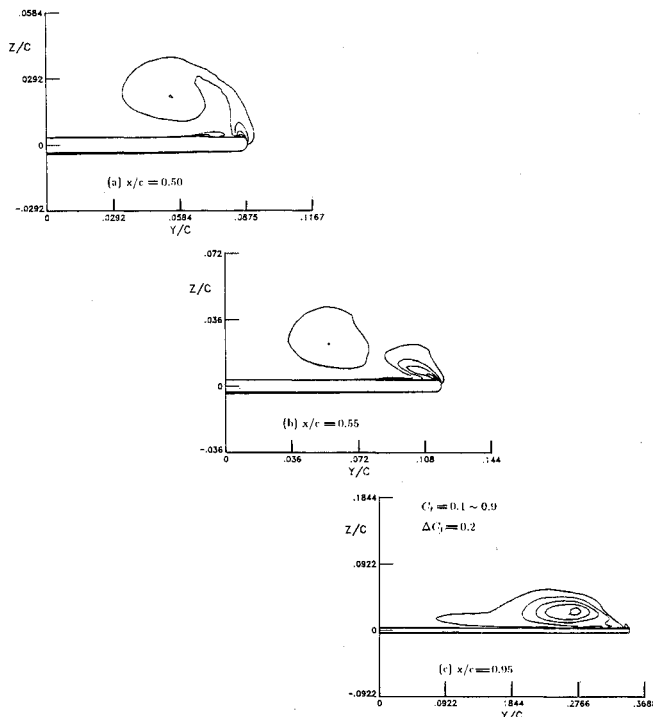


Fig. 1 Total pressure contours at  $\alpha = 12$  deg.

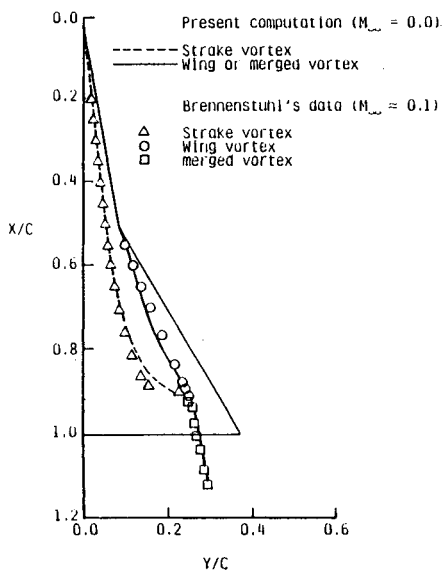


Fig. 2 Lateral positions of vortical cores at  $\alpha = 12$  deg.

$\alpha = 40$  deg reveal a clear bubble-type vortex breakdown. The breakdown zone (reversal-flow region) extends from  $x/c \approx 0.6$  to the trailing edge. Although large scale vortical structures are well simulated, further computational efforts with greater mesh resolution are needed to fully resolve the detailed structure of the vortical flow. This will, hopefully, also remove the differences between prediction and experiment in Fig. 3b and in Fig. 4 for  $\alpha = 40$  deg.

### Conclusions

The complex vortical flow over a round-edged double-delta wing has been simulated numerically by solving the incompressible Navier-Stokes equations via an upwind-relaxation finite-difference scheme. Key features of both vortical interaction and vortex breakdown are simulated. Computed lift

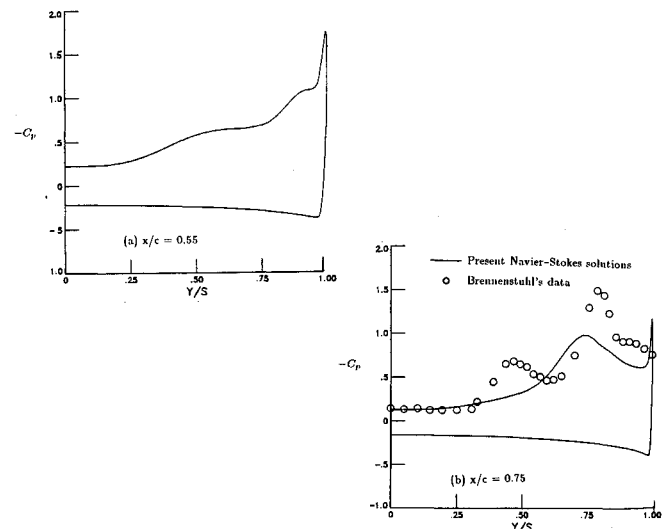


Fig. 3 Spanwise surface-pressure distributions at  $\alpha = 12$  deg ( $s$  = local semispan).

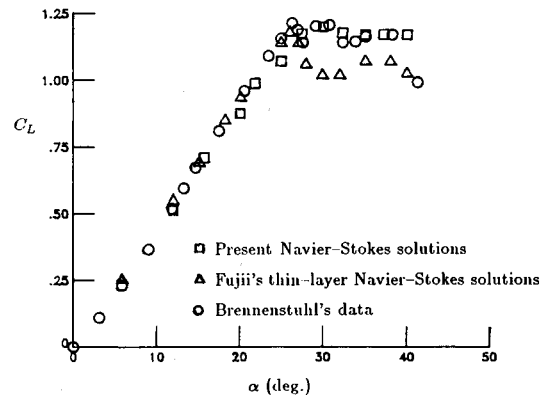


Fig. 4 Lift variation with angle of attack.

coefficients and lateral trajectories of the vortical cores are in reasonably good agreement with experimental data. Future efforts will concentrate on obtaining a better agreement between computational and experimental surface-pressure distributions.

### References

- <sup>1</sup>Brennenstuhl, U. and Hummel, D., "Vortex Formation over Double-Delta Wings," ICAS-82-6.6.3, Aug. 1982.
- <sup>2</sup>Verhaagen, N. G., "An Experimental Investigation of the Vortex Flow over Delta and Double-Delta Wings at Low Speed," AGARD-CP-342, Paper 7, April 1983.
- <sup>3</sup>Thompson, D. H., "A Visualisation Study of the Vortex Flow around Double-Delta Wings," ARL Aero-R-165, Dept. of Defense, Melbourne, Australia, Aug. 1985.
- <sup>4</sup>Fujii, K. and Schiff, L. B., "Numerical Simulation of Vortical Flows over a Strake-Delta Wing," AIAA Paper 87-1229, June 1987.
- <sup>5</sup>Hsu, C.-H., Hartwich, P.-M., and Liu, C. H., "Computation of Vortical Interaction for a Sharp-Edged Double-Delta Wing," AIAA Paper 87-0206, Jan. 1987.
- <sup>6</sup>Hsu, C.-H., Hartwich, P.-M., and Liu, C. H., "Incompressible Navier-Stokes Computations of Vortical Flows over Double-Delta Wings," AIAA Paper 87-1341, June 1987.
- <sup>7</sup>Hartwich, P.-M. and Hsu, C.-H., "High Resolution Upwind Schemes for the Three-Dimensional Incompressible Navier-Stokes Equations," AIAA Paper 87-0547, Jan. 1987.
- <sup>8</sup>Roe, P. L., "Approximate Riemann Solvers, Parameter Vectors, and Difference Schemes," *Journal of Computational Physics*, Vol. 43, 1981, pp. 357-372.